Phase relationship in the Fe-Pt-Pr ternary system at 500°C

Z. F. GU*, G. CHENG, J. REN, Z. M. WANG, H. Y. ZHOU
Department for Information Materials Science and Engineering, Guilin University of Electronic Technology, Guilin, Guangxi 541004, People's Republic of China
E-mail: gzfwzi88@gliet.edu.cn

Published online: 21 April 2006

The phase relationship in the Fe-Pt-Pr ternary system at 500°C was investigated by X-ray diffraction (XRD), scanning electron microscopy (SEM) energy dispersion spectroscopy techniques. The 500°C isothermal section consists of 13 single-phase regions, 23 two-phase regions and 11 three-phase regions. At 500°C, the maximum solid solubility of Pt in α-Fe is about 10 at.% and Fe in Pt is about 18 at.%; the maximum solubilities of Pr in α-(Fe,Pt), Fe_3Pt, FePt, $FePt_3$ and (Pt,Fe) (the solid solution of Fe in Pt) are about 6 at.% 1.5 at.% 2 at.%, 2.5 at.% and 1.5 at.%, respectively. No Pr_3Pt_4 binary compound and new ternary compounds were found.

1. Introduction

Due to the greater potential applications in the fields of microelectromechanial systems, medical instruments and high-density magnetic recording media, Fe-Pt nanocrystalline magnetic materials have attracted much attention[1–4]. The Fe-Pt, Pr-Pt, Fe-Pr binary systems bounding the Fe-Pt-Pr ternary systems has been widely investigated. In the Fe-Pt binary diagram [5], three intermetallic compounds, Fe_3Pt with $AuCu_3$ structure type, FePt with $AuCu_3$ structure type and $FePt_3$ with $AuCu_3$ structure type, have been found and formed by disorder-order phase transformation. In the Pr-Pt binary diagram [6], Seven intermetallic compounds, $PrPt_5$ with $CaCu_5$ structure type, $PrPt_3$ with Cu_2Mg structure type, $PrPt_2$ with Cu_2Mg structure type, Pr_3Pt_4 with Pd_4Pu_3 structure type, PrPt with BFe structure type, Pr_3Pt_2 with Er_3Ni_2 structure type and Pr_7Pt_3 with Fe_3Th_7 structure type, have been reported, in which $PrPt_5$, Pr_3Pt_4, Pr_3Pt_2 and Pr_7Pt_3 are formed by peritectic reaction, Pr_3Pt_4 and PrPt melt congruently. However, Ref. [7] reported that $PrPt_3$ did not exist. In the Fe-Pr binary diagram [8, 9], two intermetallic compounds, $Fe_{17}Pr_2$ with Th_2Zn_{17} structure type and Fe_2Pr with Cu_2Mg structure type, have been reported and formed by peritectic reaction. But Ref. [10] proposed that Fe_2Pr did not form in the ambient pressure. In the present paper, we will report the results of the investigation of the phase relations among the components in the Fe-Pt-Pr system at 500°C.

2. Experimental details

The phase relationship of Fe-Pt-Pr system at 500°C was constructed by using the results of the X-ray phase analysis of 65 samples, as well as that obtained from scanning electron microscopy and energy dispersion spectroscopy on some selected samples. The samples with a total mass of 1–1.5 g were prepared by arc-melting of pure metals (the purity of the ingredients was better than 99.9 wt.%) under purified argon. They were remelted not less than four times to ensure homogeneity of the constituent elements. The mass losses after the melting were less than 0.5 wt.%. After melting, all the samples were sealed in evacuated quartz tubes and homogenized at 900°C for 2 weeks, and then cooled at a rate of 10°C/min to 500°C and kept at 500°C for 4 weeks except for a small amount of samples in the Pr-Pr_7Pt_3-$Fe_{17}Pr_2$ ternary system which were homogenized only at 500°C for 30 days. After homogenizing, all ampoules with the samples were quenched in water.

The brittleness samples were grinded into powders in porcelain mortar for X-ray diffraction. A few toughness samples were pressed into slices (7 mm × 3 mm × 1 mm) and sealed again in quartz tubes, then annealed under the protection of purified argon at 500°C for a week to eliminate the stress and quenched in water for X-ray diffraction. Phase analysis was carried out using X-ray diffraction (CuKα radiation), scanning electron microscopy and energy dispersion spectroscopy techniques.

*Author to whom all correspondence should be addressed.
0022-2461
DOI: 10.1007/s10853-006-7001-1

3. Results and discussion

3.1. Compounds of Pr_3Pt_4 and Fe_2Pr

Results of X-ray diffraction confirm the existence of $PrPt_5$, $PrPt_3$, $PrPt_2$, PrPt Pr_3Pt_2 and Pr_7Pt_3 six compounds in Pr-Pt binary system, but Pr_3Pt_4 compound was not found. Fig. 1 displays the XRD pattern for the Pr_3Pt_4 sample. From these data, it follows that the Pr_3Pt_4 sample consists of two phases PrPt and $PrPt_2$. This means that no Pr_3Pt_4 compound form at 500°C, and it has decomposed totally into the two neighboring compounds PrPt and $PrPt_2$. The reason for this is not fairly clear but we think it is likely related to the specific structural stability of this type of compounds R_3Pt_4 for which the atomic radius ratio r_R/r_{Pt} has to fall within 1.25–1.35 [11].

Ref. [8, 9] reported that Fe_2Pr compound formed by peritectic reaction, $Fe_{17}Pr_2 + L \rightarrow Fe_2Pr$ at 1000°C. We prepared a series of samples in the phase range including Fe_2Pr compound of Fe-Pr binary system. These samples were annealed at 500°C for 30 days, and some for 60 days. The XRD analysis showed that all the presently investigated samples are composed of $Fe_{17}Pr_2$ and Pr, no Fe_2Pr compound was found under our experimental conditions, which is agreement with the report in Ref. [10].

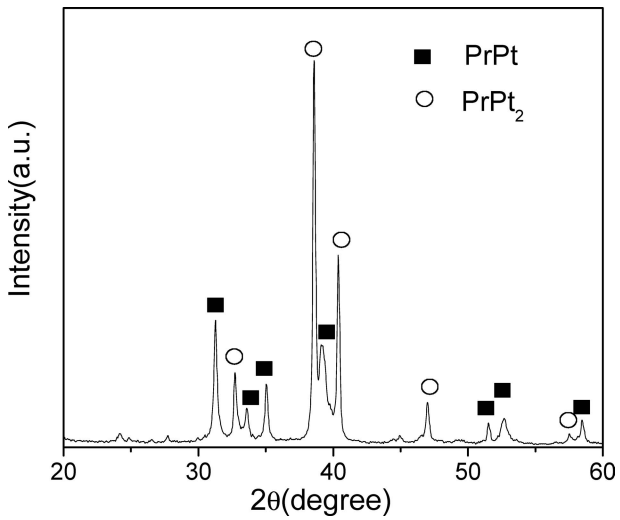

Figure 1 The XRD pattern of the Pr_3Pt_4 sample annealed at 500°C.

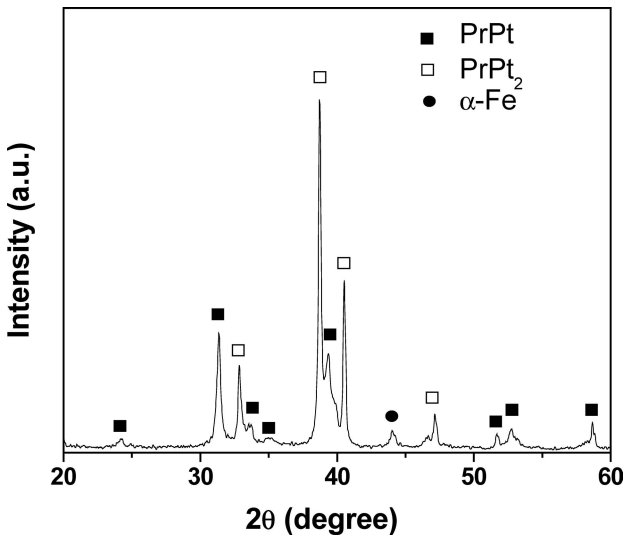

Figure 2 The XRD pattern of the $Fe_{50}Pt_{30}Pr_{20}$ sample annealed at 500°C.

3.2. Solid solubility

By using X-ray diffraction, scanning electron microscopy and energy dispersion spectroscopy techniques, we have observed, at 500°C, that the maximum solid solubility of Pt in α-Fe is about 10 at.%, the maximum solubility of Fe in Pt is about 18 at.%. The single phase ranges of α-(Fe,Pt), Fe_3Pt, FePt, $FePt_3$ and (Pt,Fe) are from 0 to 10 at.%Pt, 14 to 31 at.%Pt, 33 to 63 at.%Pt, 66 to 79 at.%Pt, and 82 to 100 at.%Pt, respectively. It is interesting that no solubility of Pr in both α-Fe and Pt was reported [6, 8, 9], but in this work, the maximum solubilities of Pr in α-(Fe,Pt) and (Pt,Fe) solid solution were found to be about 6 at% and 1.5 at.%, respectively, and they are about 1.5 at.% 2 at.% and 2.5 at.%, respectively, with Pr in Fe_3Pt, FePt, and $FePt_3$.

3.3. Isothermal section at 500°C

By comparing and analyzing the X-ray diffraction patterns of 65 samples, together with the results obtained from scanning electron microscopy and energy dispersion spectroscopy on some of the selected samples. We have determined the phase compositions of each sample. Results of XRD measurements on the sample of $Fe_{50}Pt_{30}Pr_{20}$ ternary alloy are displayed in Fig. 2. These

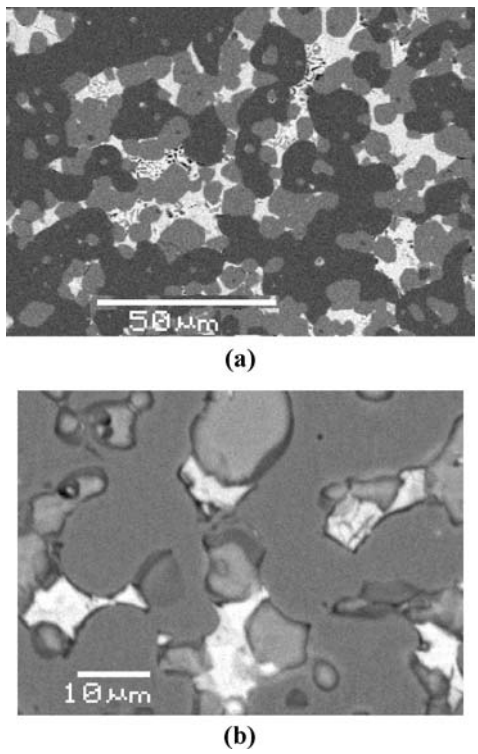

Figure 3 (a) SEM micrograph of the $Fe_{86}Pt_3Pr_{11}$ sample annealed at 500°C. (b)SEM micrograph of the $Fe_{56}Pt_{40}Pr_4$ sample annealed at 500°C.

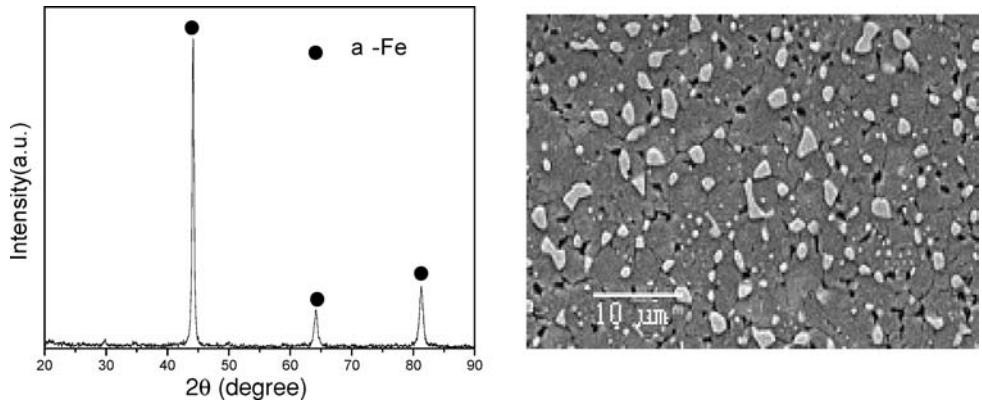

Figure 4 The XRD pattern (left) and SEM micrograph (right) of the $Fe_{88}Pt_{10}Pr_2$ sample annealed at 500°C.

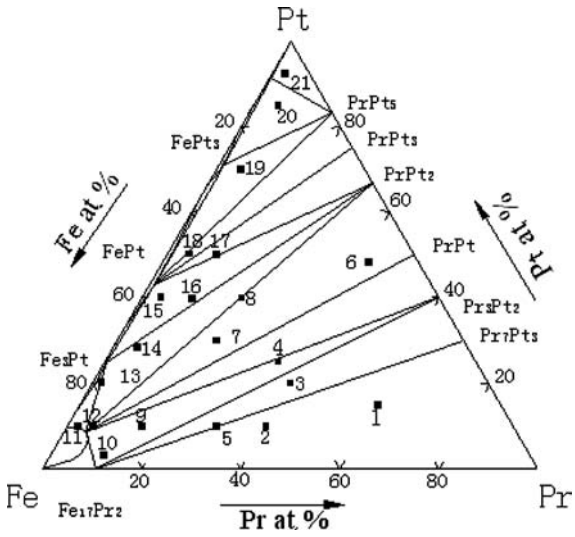

Figure 5 Isothermal section of the Fe-Pt-Pr ternary phase diagram at 500.

data indicate that are displayed in Fig.2 it is a three-phase alloy consisting of PrPt, $PrPt_2$ and α-Fe,and they are also a clear proof that Pr_3Pt_4 compound does not exist, otherwise the Pr_3Pt_4 phase should appear in this sample. Scanning electron micrographs showing the microstructures of the samples of $Fe_{86}Pt_3$ Pr_{11} and $Fe_{56}Pt_{40}Pr_4$ are represented in Fig. 3 (a) and Fig. 3 (b), respectively. One can visualize that they are all the three-phase samples in which the former consists of α-(Fe, Pt), $Fe_{17}Pr_2$ and Pr_3Pt_2 and the latter FePt, Fe_3Pt and $PrPt_2$. However, the X-ray diffraction data show that they are the two-phase alloys consisting of α-(Fe, Pt) and $Fe_{17}Pr_2$, and FePt and Fe_3Pt, respectively, without the observation of the presence of the minor phases Pr_3Pt_2 or $PrPt_2$. The reason for this is due to the fact that often the presence of a small amount of phase of less than 5% is hard to be detected by means of XRD measurements. The similar results are also observed in Fig. 4 in which the XRD pattern (left part) for the sample $Fe_{88}Pt_{10}Pr_2$ reveals it is a single phase of α-(Fe, Pt), but in fact there exists a small amount of second phase of Fe_3Pt according to the SEM micrograph (right part). Consequently, this sample is identified as a mixture of two-phase α-(Fe, Pt) and Fe_3Pt coexisting, but close to the phase-boundary between the α-(Fe, Pt) and Fe_3Pt. The results of the phase analysis for the aforementioned samples and the other selected samples are listed in Table I.

On basis of all the results obtained for the presently investigated samples, the phase relationship of Fe-Pt-Pr ternary system at 500°C was established. The experimental Fe-Pt-Pr ternary diagram at 500°C, as presented in Fig. 5, shows it consists of 13 single-phase regions, 23 two-phase regions and 11 three-phase regions.

The 13 single-phase regions are: α (α-Fe), β(Fe_3Pt), γ(FePt), δ($FePt_3$), ε(Pt), ζ($PrPt_5$), η($PrPt_3$), θ($PrPt_2$), ι(PrPt), κ(Pr_3Pt_2), λ(Pr_7Pt_3), μ(Pr), ν($Fe_{17}Pr_2$).

The 23 two-phase regions are: $\alpha+\beta$, $\beta+\gamma$, $\gamma+\delta$, $\delta+\varepsilon$, $\varepsilon+\zeta$, $\zeta+\eta$, $\eta+\theta$, $\theta+\iota$, $\iota+\kappa$, $\kappa+\lambda$, $\lambda+\mu$, $\mu+\nu$, $\nu+\alpha$, $\nu+\lambda$, $\nu+\kappa$, $\alpha+\kappa$, $\alpha+\iota$, $\alpha+\theta$, $\beta+\theta$, $\gamma+\eta$, $\gamma+\zeta$, $\delta+\zeta$.

The 11 three-phase regions are: $\lambda+\mu+\nu$, $\lambda+\nu+\kappa$, $\alpha+\nu+\kappa$, $\alpha+\kappa+\iota$, $\alpha+\theta+\iota$, $\alpha+\beta+\theta$, $\beta+\gamma+\theta$, $\gamma+\eta+\theta$ $\gamma+\zeta+\eta$, $\gamma+\delta+\zeta$, $\delta+\varepsilon+\zeta$.

TABLE I. Identification of phase for the selected ternary alloys at 500°C

Samples	Ternary alloys	Phase components
1	$Fe_{25}Pt_{15}Pr_{60}$	$Fe_{17}Pr_2+Pr_7Pt_3+Pr$
2	$Fe_{50}Pt_{10}Pr_{40}$	$Fe_{17}Pr_2+Pr_7Pt_3+Pr$
3	$Fe_{40}Pt_{20}Pr_{40}$	$Fe_{17}Pr_2+Pr_3Pt_2+Pr_7Pt_3$
4	$Fe_{40}Pt_{25}Pr_{35}$	α-Fe + $Fe_{17}Pr_2+Pr_3Pt_2$
5	$Fe_{60}Pt_{10}Pr_{30}$	$Fe_{17}Pr_2+Pr_7Pt_3$
6	$Fe_{10}Pt_{48}Pr_{42}$	α-Fe + PrPt + $PrPt_2$
7	$Fe_{50}Pt_{30}Pr_{20}$	α-Fe + PrPt + $PrPt_2$
8	$Fe_{40}Pt_{40}Pr_{20}$	α-Fe + $PrPt_2$
9	$Fe_{75}Pt_{10}Pr_{15}$	α-Fe + $Fe_{17}Pr_2+Pr_3Pt_2$
10	$Fe_{86}Pt_3$ Pr_{11}	α-Fe + $Fe_{17}Pr_2+Pr_3Pt_2$
11	$Fe_{88}Pt_{10}Pr_2$	α-Fe + Fe_3Pt
12	$Fe_{85}Pt_{10}Pr_5$	α-Fe + $PrPt_2$
13	$Fe_{78}Pt_{20}Pr_2$	α-Fe + Fe_3Pt
14	$Fe_{67}Pt_{28}Pr_5$	α-Fe + Fe_3Pt + $PrPt_2$
15	$Fe_{56}Pt_{40}Pr_4$	FePt + Fe_3Pt + $PrPt_2$
16	$Fe_{50}Pt_{40}Pr_{10}$	FePt + Fe_3Pt + $PrPt_2$
17	$Fe_{40}Pt_{50}Pr_{10}$	FePt + $PrPt_2$
18	$Fe_{45}Pt_{50}Pr_5$	FePt + $PrPt_5$
19	$Fe_{25}Pt_{70}Pr_5$	FePt + $FePt_3$ + $PrPt_5$
20	$Fe_{10}Pt_{85}Pr_5$	Pt + $FePt_3$ + $PrPt_5$
21	$Fe_5Pt_{92}Pr_3$	Pt + $PrPt_5$

4. Conclusion

1. The 500°C isothermal section of the ternary Fe-Pt-Pr system excludes the possibility of the presence of the Pr_3Pt_4 phase although it is present at 900°C and 300°C, respectively.

2. The maximum solid solubility of Pt in α-Fe is about 10 at.%; the maximum solubility of Fe in Pt is about 18 at.%. The single phase ranges of α-(Fe,Pt), Fe_3Pt, FePt, $FePt_3$ and (Pt,Fe) are from 0 to 10 at.%Pt, from 14 to 31 at.%Pt, from 33 to 63 at.%Pt, from 66 to 79 at.%Pt, from 82 to 100 at.%Pt, respectively. The maximum solubilities of Pr in α-(Fe,Pt), Fe_3Pt, FePt, $FePt_3$ and (Pt,Fe) is about 6 at.% 1.5 at.% 2 at.% 2.5 at.% and 1.5 at.%, respectively.

3. The isothermal section of the Fe-Pt-Pr ternary phase diagram at 500°C consists of 13 single-phase regions, 23 two-phase regions, and 11 three-phase regions. No new ternary compounds was found.

Acknowledgements

This work was supported by the National Natural Science Foundation of China (Grant No: 50261002)

References

1. E. BRUCK, Q. F. XIAO, P. D. THANG, M. J. YOONEN, F. R. DE. BOER and K. H. J. BUSCHOW, *Physica B.* **300** (2001) 215.
2. J. P. LIU, Y. LIU, C. P. LUO, Z. S. SHAN and D. J. SELLMYER, *J. Appl. Phys.* **81** (1997) 5644.
3. B. M. LAIRSON, M. R. VISOKAY, R. SINELAIR and B. M. CLEMENS, *J. Appl. Phys. Lett.* **62** (1993) 639.
4. M. WATANABE and M. H. MMA, *JAN. [J]. J. Appl. Phys. (Part2)* **35** (1996) 1264.
5. T. MASSALSKY (Ed.), Binary Alloy Phase Diagrams, 2nd ed, (ASM International, Materials Park, OH, 1996).
6. KUBASCHEWSKI, Binary Alloy Phase Diagrams, 2nd ed, (ASM International, Materials Park, OH, 1997) pp 1572.
7. I. R. HARRIS, *J. Less-Common Met.* **24** (1968) 459.
8. MOFFAT, Binary Alloy Phase Diagrams, 2nd ed (ASM International, Materials Park, OH, 1997) p 3089
9. Y. H. ZUANG, H. Y. ZHOU and J. X. ZHEN, *Acta Metallurgica Sinica* **23** (1987) B42
10. W. ZHANG, C. LI and X. SU, *Journal of Phase Equilibria* **2** (1999) 158.
11. A. PALENZONA, *J. Less-Common Met.* **53** (1977)133.

Received 3 February
and accepted 6 September 2005